Influence of Grain Refiners on the Wettability of Al_2O_3 Substrate by Aluminum Melt

JIAWEI YANG, SARINA BAO, SHAHID AKHTAR, PING SHEN, and YANJUN LI

It is well known that grain refiner additions in aluminum melts significantly reduce the filtration efficiency of ceramic foam filters (CFF). However, the mechanism remains unclear. In this work, the influence of grain refiners on the wettability of alumina substrate by aluminum melt was studied by both conventional sessile drop and improved sessile drop methods at different temperatures and vacuums. Commercial purity aluminum (CP-Al) and grain refiner master alloys Al-3Ti-1B, Al-5Ti-1B, Al-3Ti-0.15C were used. It is found that master alloy melts wet alumina substrate better than CP-Al. Generally, a lower temperature or lower vacuum results in a higher contact angle. The roles of grain refiner particles in improving the wettability were studied by analyzing the solidification structure of post wetting-test droplets using SEM. Strong sedimentation of grain refiner particles at the metal-substrate interface was observed, which is attributed to the higher density of grain refiner particles compared to the Al melt. Meanwhile, a large fraction of grain refiner particles agglomerates at the oxide skin of the aluminum droplets, showing a strong adhesion between the particles and oxide skin. Such adhering of grain refiner particles is proposed to enhance the rupture of the original oxide skin of the droplets and slow down the reoxidation process at the surface layer. Both adherence of grain refiner particles to surface oxide skin and sedimentation of particles at the metal-substrate interface are responsible for the wetting improvement.

https://doi.org/10.1007/s11663-020-01989-4

I. INTRODUCTION

FILTRATION by ceramic foam filter (CFF) is an efficient, cheap, and popular way to remove inclusions from aluminum melt in order to increase metal quality. Filtration mechanism has been investigated by many researchers.[1–13] Massive progress has been made in understanding the influences of flow rate,[2] filter position,[14] filtration time,[15] filter types and filter surface treatment[5,8,15–19] on the filtration behavior. Bao *et al.*[20] studied the effect of the wetting properties between filter-melt and melt-inclusion on filtration behavior. It is proposed that a good wetting between the melt and filter as well as a poor wetting between melt and inclusions would increase the possibility that inclusions hit the inner wall of CFF and be captured.[3] However, Voigt *et al.*[21] pointed out that the higher the contact angle between filter and melt, the higher filtration efficiency can be achieved. They also concluded that the rough surface of the filter wall improves the filtration efficiency. The rough surface inside the filter increases the melt flow resistance, where inclusions have a higher chance of hitting the porous wall. Therefore the chance for them to be caught and remain on the wall increases.[22]

Nowadays, grain refiners, for example Al-Ti-B and Al-Ti-C master alloys, are often added into aluminum melt to refine the grain structure by increasing the number of nucleation sites during solidification. It is expected that the casting quality can be further improved with the combination of inoculation by grain refiners and CFF filtration. However, the addition of grain refiners was found to significantly reduce the filtration efficiency under high inclusion load.[13,23–26] One of the hypotheses suggested that the reduced filtration efficiency was due to the prevention or destruction of the inclusion bridge inside the filter by grain refiner particles. Unfortunately, no convincing experimental evidence has been revealed to show how and why the grain refiners could damage or prevent the formation of bridge. Another possible reason for the reduction of filtration efficiency could be the change of wettability between Al melt and CFF by addition of grain refiner master alloys.

JIAWEI YANG and YANJUN LI are with the Norwegian University of Science and Technology, 7491 Trondheim, Norway. Contact e-mail: yanjun.li@ntnu.no SARINA BAO is with the SINTEF Industry, 7465 Trondheim, Norway. SHAHID AKHTAR is with the Research and Development Karmøy, Norsk Hydro, 4265 Håvik, Norway. PING SHEN is with the School of Materials Science and Engineering, Jilin University, Changchun 130022, P.R. China.

Manuscript submitted May 17, 2020; accepted September 23, 2020.

Published online: 20 November 2020

Al-Ti-B and Al-Ti-C master alloys contain TiB_2 or TiC particles and Al_3Ti intermetallic phase. Experimental results have shown that Al_3Ti alone in aluminum melt does not affect the filtration efficiency.[24] It is well known that TiB_2 wets well with the molten Al. Weirauch *et al.*[27] showed that the contact angle between a pure polished TiB_2 and Al melt can be as low as 0 deg after 17 hours holding under a high vacuum at 1025 °C. With the presence of 1 to 2 wt pct C in TiB_2, the contact angle can still be as good as 9 to 12 deg in vacuum at 1025 °C. Lin *et al.*[28] reported a final equilibrium contact angle of 12 to 17 deg at 850 °C to 1050 °C for liquid Al on $TiC_{0.7}$ substrate, which indicates a good wetting between Al and TiC as well. On the contrary, Al_2O_3 does not wet Al melt well. The measured contact angles between Al_2O_3 and Al vary from 60 to 167 deg at 700 °C to 1400 °C in various literature.[29–38] The large scatter in measured contact angle values is due to different test methods, vacuum states, temperatures, sample purities, *etc*. It is important to point out that Al oxidizes easily, even at 10^{-49} bar partial pressure at 700 °C.[31] The oxide-free Al droplet may oxidize again even in a high vacuum[39] after the primary oxide film has been removed. For the wetting test between ceramics and molten Al, a high vacuum and a temperature higher than 950 °C are usually preferred. Below that temperature, a large contact angle is usually encountered because of the presence of the oxide film.[32] So far, how grain refiner particles influence the wettability of Al melt to Al_2O_3 substrate of CFF is not known yet.

In the present work, the influence of grain refiners on wetting of aluminum melt on pure alumina substrate was investigated using both conventional sessile drop[31] method at 1100 °C with a vacuum of 3×10^{-4} Pa and an improved sessile drop method[40,41] at 1000 °C with a vacuum of 1×10^{-3} Pa. A combination of the two wetting test methods is expected to give more comprehensive results of the wetting behavior. The possible mechanism on how grain refiner particles change the wettability between Al and alumina filter was also discussed.

Table I. Chemical Compositions of Materials

Elements (Wt Pct)	Si	Fe	Ti	B	C	Al
CP-Al	0.06	0.06	0.01			bal.
Al-3Ti-1B			3	1		bal.
Al-5Ti-1B			5	1		bal.
Al-3Ti-0.15C			3		0.15	bal.

II. EXPERIMENTAL

A. *Materials*

The experimental materials used in this work were CP-Al and master alloys Al-3Ti-1B, Al-5Ti-1B, Al-3Ti-0.15C, together with 99.7 pct pure alumina substrate. The chemical compositions of materials are listed in Table I. The weight of the aluminum samples was 0.037 ± 0.003 g. The average surface roughness (R_a) was 0.7 and 1 μm for the alumina disk in the conventional and improved sessile drop tests, respectively. R_a is the arithmetic average of the absolute values of the roughness profile along the sampling length at the sample surface. It is determined from the deviations about the centerline within the evaluation length. These values were measured by a light microscopy (InfiniteFocus, Alicona, Raaba/Graz, Austria) over 3 mm distance.

Two types of wetting tests, conventional sessile drop test and improved sessile drop test were conducted. An overview of the experiments was listed in Table II.

B. *Conventional Sessile Drop Test*

The conventional sessile drop test was conducted at Norwegian University of Science and Technology (NTNU). The substrates and samples were first cleaned in acetone assisted by ultrasonic vibration for 7 minutes. Then, the substrate together with the Al sample putting on a graphite sample holder was inserted into the furnace (Figure 1) surrounded by graphite heating elements, which are located in a water-cooled vacuum chamber. After the sample was sent into the chamber, the chamber was enclosed and sealed to ensure that a high vacuum can be established in the chamber. A calibrated k-type thermocouple was placed just below the substrate to monitor the temperature. The samples were first heated to 900 °C with a heating rate of 300 °C/min, and then heated up to 1100 °C with a constant rate of 50 °C/min in a high vacuum of 3×10^{-4} Pa and then held for 1 hour. A high-resolution camera (Sony XCD-SX910CR, Sony, Millersville) was utilized to take images with a frequency of 6 pictures/min. The shape

Table II. Experimental Overview

	Conventional Sessile Drop Method	Improved Sessile Drop Method
Temperature (°C)	1100	1000
Sample	CP-Al, Al-3Ti-1B, Al-5Ti-1B, Al-3Ti-0.15C	CP-Al, Al-3Ti-1B, Al-5Ti-1B, Al-3Ti-0.15C
Substrate	$\phi 10 \times 3$ mm^3 pure alumina disk	$20 \times 20 \times 3$ mm^3 pure alumina
Vacuum (Pa)	3×10^{-4}	1×10^{-3}
Software for Contact Angle Analysis	Fta32	axisymmetric drop-shape-analysis program (ADSA)

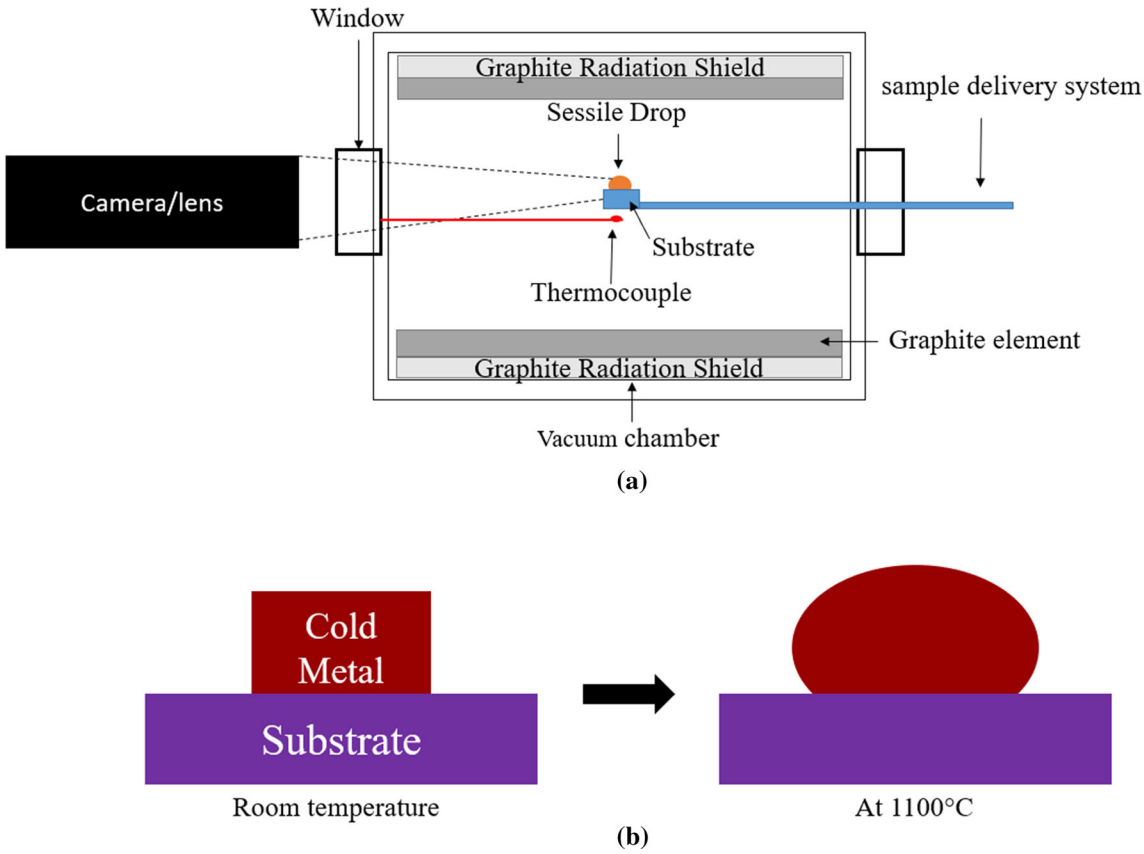

Fig. 1—(*a*) A sketch of the conventional sessile drop furnace. (*b*) A sketch of the conventional sessile drop method, where the cold metal and cold substrate were heated together in the chamber.

and size evolution of the sample, as well as the wetting behavior, can be directly observed during the experiments owing to the self-illumination of samples.

C. *Improved Sessile Drop Test*

The improved sessile drop test was conducted at Jilin University. The same substrate and sample cleaning process as in the previous test was also applied. The chamber with the substrate was evacuated to 1×10^{-3} Pa and heated up to 1100 °C with a heating rate of 20 °C/min. It was held at 1100 °C for 10 minutes for further cleaning of the substrate surface before the temperature was lowered back to the target temperature, 1000 °C. Such a procedure has been used by other authors before for keeping the high vacuum as well as to remove the substrate surface contaminants.[28,42] Then, the cold metal was delivered through an alumina tube to the substrate surface and then melted immediately, as described in a schematic drawing in Figure 2. The thermocouple used is a W5-type (W-5 pct Ra/W-26 pct Rh) thermocouple. A charge-coupled device (CCD) camera was used to take pictures from the moment that the sample touched the substrate, which is defined as time zero. Extremely fast heating of metal could help to remove the surface oxide layer, and the pre-contact between the metal and substrate was avoided by this method. Laser illumination[43] was applied in this type of wetting tests instead of self-illumination used by the conventional sessile drop method, giving less scattering of the measured contact angles. The drawback of this method is, however, that the sample surface condition cannot be directly observed. More details about the experimental procedure and equipment can be found in the literature.[41]

After wetting experiments, the solidified aluminum droplets together with the substrate were embedded in epoxy resin, cut, and mechanically polished. The microstructure at the cross-section of the droplet and substrate was characterized by a scanning electron microscope (SUPRA 55-VP, Zeiss, Oberkochen, Germany) equipped with an energy-dispersive spectrometer (Octane, EDAX, Mahwah). An accelerating voltage of 15 kV and a working distance of 10 mm were applied in the SEM observation.

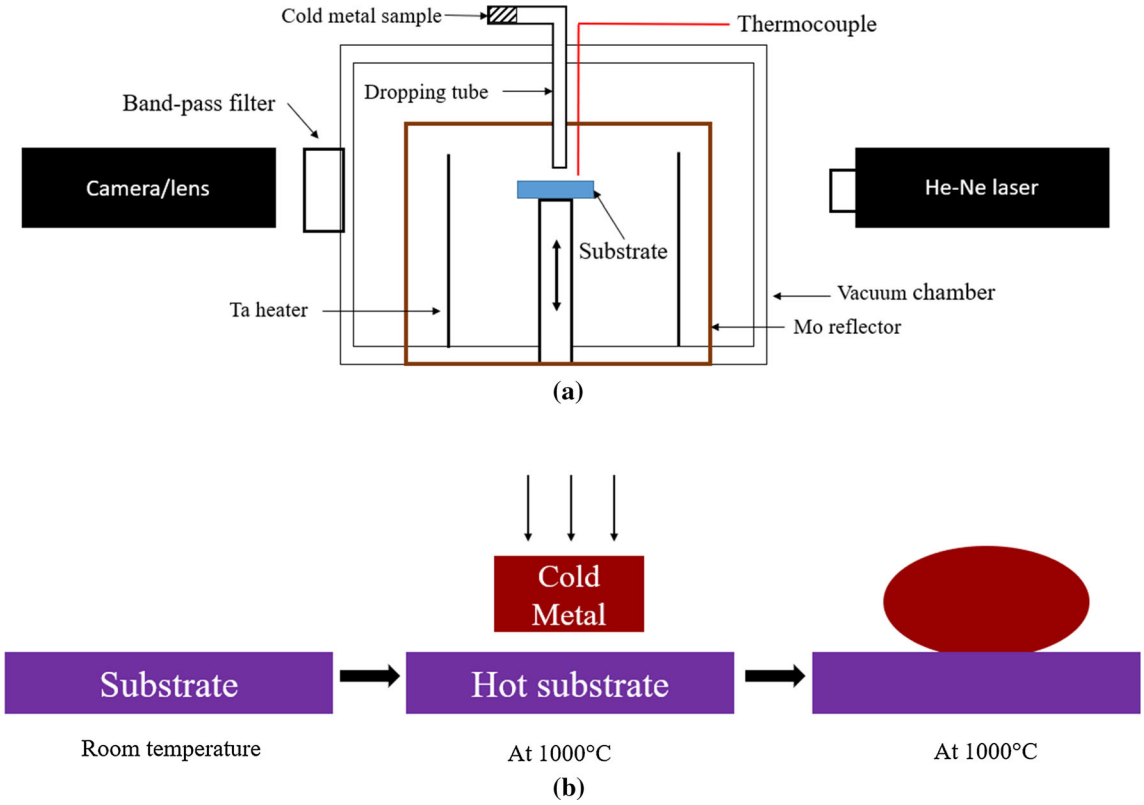

Fig. 2—(*a*) A sketch of the improved sessile drop furnace. (*b*) A sketch of the improved sessile drop method where the cold metal drops onto a hot substrate and melts immediately.

III. RESULTS

A. *Contact Angle Evolution During Conventional Sessile Drop Test*

The evolution of the contact angle between the droplets of different aluminum alloys and pure alumina substrate is shown in Figure 3, where the heating curve is also depicted. Note that time zero is given as when the furnace heating was started, and the contact angle is measured once the solid metal sample is changed into a spherical droplet. As a general trend, the contact angle decreases with time in the high vacuum of 3×10^{-4} Pa in this case. The final contact angle on pure alumina is 89 deg for CP-Al, 83 deg for Al-5Ti-1B master alloy, 82 deg for Al-3Ti-1B, and 79 deg for Al-3Ti-0.15C. The master alloys show a relatively lower contact angle than CP-Al. Furthermore, a faster decrease of contact angle can be seen for all master alloys.

Figure 4 compares the dynamic surfaces evolution of droplets on pure alumina. Floating oxide skin can be seen on the surface of all droplets (pointed by arrows) after 6 minutes at approximately 1000 °C (Figures 4(a) through (d)). The oxide skin of master alloy droplets cracks, while it distributes more evenly on the CP-Al sessile drop. Figures 4(e) and (f) show the droplets of different alloys at the temperature of 1100 °C. A clean surface can be observed for the droplets of all master alloys, while some oxide skin patches are still floating on the CP-Al droplet surface.

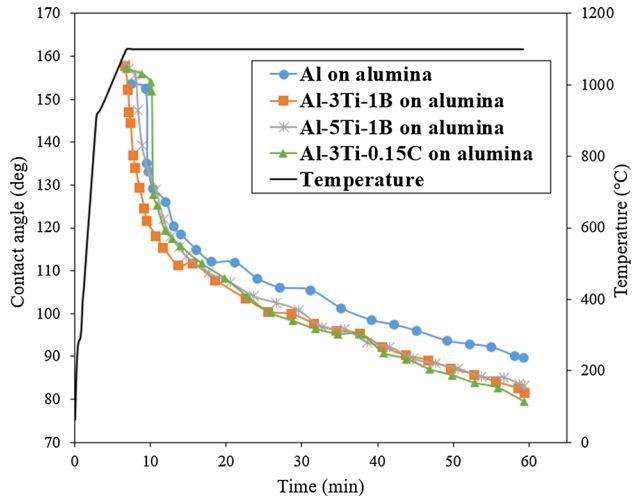

Fig. 3—The contact angle of Al and master alloys on pure alumina. The time zero is given when the furnace heating started, and the contact angles measured once the melted Al forms a spherical shape.

B. *Contact Angle Evolution During Improved Sessile Drop Test*

Generally, a similar exponential decay trend of contact angle was observed during isothermal heating in the improved sessile drop test, as indicated in Figure 5 at 1000 °C. However, samples become spherical immediately after touching the substrate. A sharper

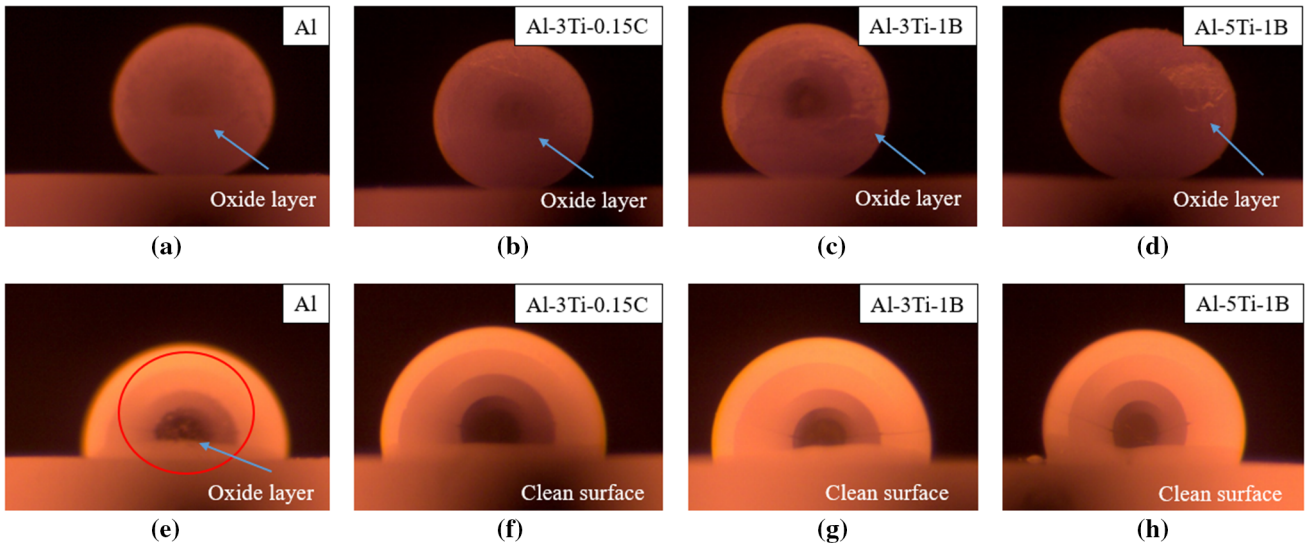

Fig. 4—Sessile drops on pure alumina during the conventional sessile drop test. (*a*) to (*d*) approximately at 1000 °C after 6 min heating, (*e*) to (*h*) at 1100 °C after 12 min heating.

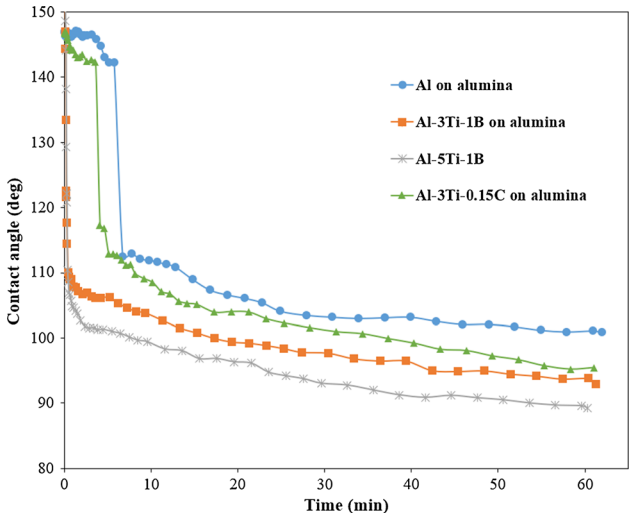

Fig. 5—The contact angle of Al and master alloys on pure alumina at 1000 °C by improved sessile drop method in the vacuum of 1×10^{-3} Pa. Time zero is set when the cold metal falls on the substrate.

descending of the contact angle with time than conventional sessile drop tests can be observed. For example, it takes more than 14 minutes to decrease until contact angle of 110 deg in the conventional method (Figure 3), while only less than 12 minutes in improved method: within approximately 30 seconds for the Al-5Ti-1B and Al-3Ti-1B master alloys, and 8 and 12 minutes for the Al-3Ti-0.15C master alloy and CP-Al, respectively. This is because the cold metal drops on the hot substrate and melts immediately, without forming more continuous oxide skin on the surface of droplets during the heating process. As expected, a slightly higher final contact angle was observed at the lower temperature of 1000 °C with the same holding period; *i.e.*, 99 deg for CP-Al, and 94 deg for Al-3Ti-0.15C, 89 deg for Al-3Ti-1B, and 87 deg for Al-5Ti-1B on alumina, than those at 1100 °C measured with the conventional sessile drop method. Still, CP-Al shows a higher contact angle than the rest of the grain refiner master alloys and a slower deoxidation process at the beginning period as shown in Figure 5. No dynamic surface behavior could be observed with the laser illumination mode in the present improved sessile drop test, especially due to the instant deoxidation process.

C. *Microstructures of Solidified Droplets*

As shown in Figure 6, the solidified droplet contains long rod-like Al_3Ti intermetallic phase, Al-Fe-Si intermetallic phase along grain boundaries, and small TiB_2 particles. Interestingly, the lower part and the top part of the droplet show different solidification structures: a large fraction of bright particles distribute in the shape of networks in the lower part, while the top part is relatively cleaner. A careful examination by EDS shows that grain boundaries in the upper part are mainly composed of Al-Fe-Si intermetallic particles (Figure 6(c)). In the lower part, the network structures are composed of agglomerated TiB_2 particles (Figure 6(f)) together with Al-Fe-Si intermetallic phase. This indicates that a TiB_2 particle depleted zone is formed in the upper part after the TiB_2 particles sedimented into the bottom of the droplet. Surprisingly, TiB_2 particles are also found agglomerating along the droplet surface regardless of the height (Figure 6(b)), which is opposite to their sedimentation nature. Figure 6(d) shows the interface between the droplet and the Al_2O_3 substrate. Besides sedimentation of TiB_2 particles at the interface, no reaction layer can be seen. However, the aluminum melt and TiB_2 particles that penetrated the cavity of the substrate can be observed. Figure 6(a) shows the triple line between the droplet and substrate, where an agglomeration of TiB_2 particles can also be observed.

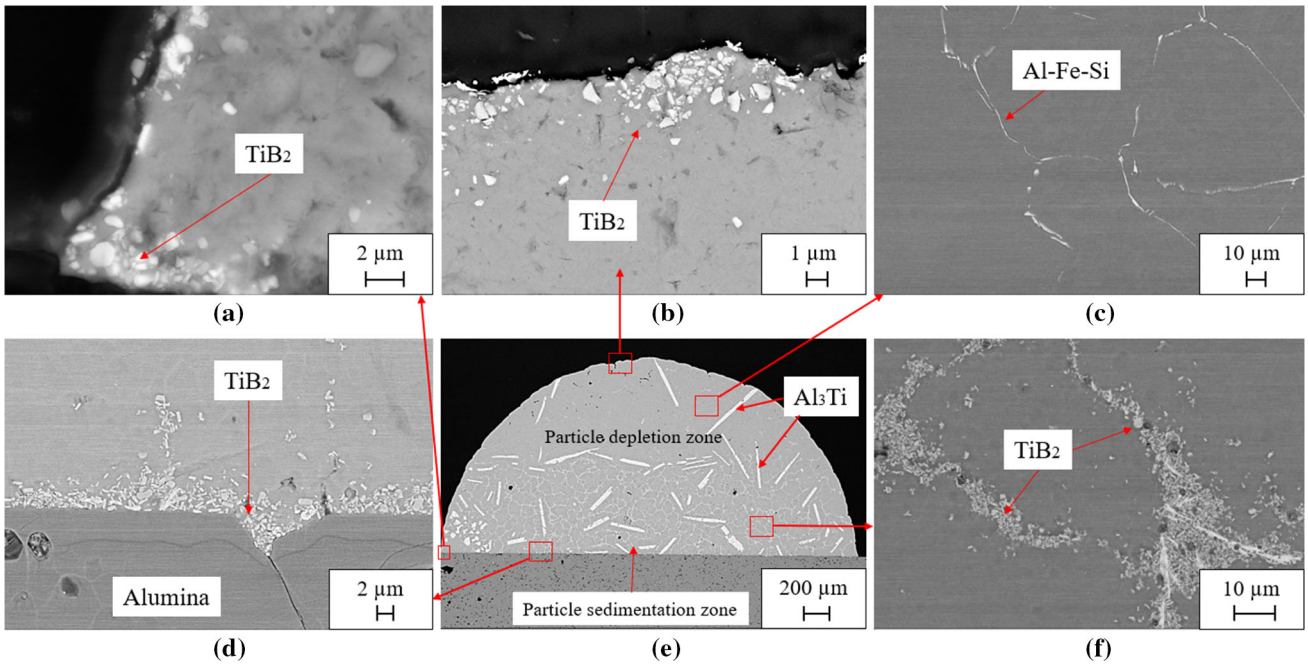

Fig. 6—The microstructure of Al-5Ti-1B master alloy on the alumina after 1 h holding at 1000 °C in high vacuum. (*a*) A magnified area at the corner where TiB_2 particles agglomerated at the triple line. (*b*) Magnified top side of the periphery of the droplet where TiB_2 particles are agglomerated. (*c*) Magnified area in particle depletion zone where only Al-Fe-Si intermetallic phase is found along grain boundaries. (*d*) The interface between alumina substrate and master alloy, where TiB_2 agglomerates and settles onto the substrate. Meanwhile, no reaction but penetration of aluminum into the substrate is observed. (*e*) Macrostructure of solidified sessile droplet on alumina. (*f*) A magnified area in particle sedimentation zone where massive TiB_2 particles are agglomerated along grain boundaries.

Similar microstructures are detected for the solidified droplet of Al-3Ti-1B by both conventional and improved sessile drop tests.

As shown in Figure 7, similar to Al-Ti-B droplet samples, Al-3Ti-0.15C master alloy also shows the sedimentation and depletion zones of TiC particles, long needle shaped Al_3Ti particles and grain boundary Al-Si-Fe intermetallic particles. The black pits in the sample are pores forming during mechanical polishing. As can be seen, TiC particles not only settle down on the surface of the substrate (Figure 7(d)), but also agglomerate and distribute along the oxide skin at the periphery of the droplet (Figures 7(a) and (b)), regardless of the height. In the sedimentation zone at the lower part of the droplet, the fine TiC particles agglomerate along the grain boundaries (Figure 7(f)) forming a network structure. Nearly no TiC particles can be observed along grain boundaries in the depletion zone in the upper part of the droplet, where Al-Fe-Si intermetallic phase precipitates along grain boundaries. Note that the number density of TiC particles is smaller than that of TiB_2 particles.

IV. DISCUSSION

A. *Influence of Grain Refiner Particles on Contact Angle*

The wetting tests with both conventional sessile drop (Figure 3) and improved sessile drop (Figure 5) methods show that the contact angles between liquid aluminum containing grain refiner particles (master alloys) and alumina are lower than those of pure Al. In principle, the liquid-solid contact angle can be affected by several factors such as heterogeneity of the substrate surface, temperature, trace elements in the alloy, vacuum, liquid properties (viscosity, surface tension), *etc*. For the present work, the parameters such as substrate surface roughness, droplet weight, temperature, time, vacuum state are strictly controlled. This ensures that the change of contact angle is mainly dependent on the alloy parameters. In addition, the evaporation of liquid Al during the wetting experiment is unavoidable and will also have a significant effect on the contact angle evolution.

High vacuum and high temperatures are vital to get fresh metal-solid contact during the wetting test. However, the contact angle can be underestimated due to the evaporation of liquid Al in vacuum.[44] In principle, the droplet height (H) will reduce while the base diameter (D) of the droplet will either stay constant or reduce for pure evaporation process (no wetting involved). In the present case, metal droplet spreads while the height reduces (Figure 8). This indicates a wetting process rather than a pure evaporation process. The master alloys have larger D/H values than CP-Al. This indicates a better wetting of master alloys to the substrate. Meanwhile, the D/H values of Al-Ti-B samples are larger than Al-Ti-C sample. The diameters increase with time and are almost stabilized after 1 hour holding time, while the height decreases and is almost stabilized at the end for all samples. This indicates that the dynamic wetting properties stabilize as well, where the final contact angle is representative for the current system.

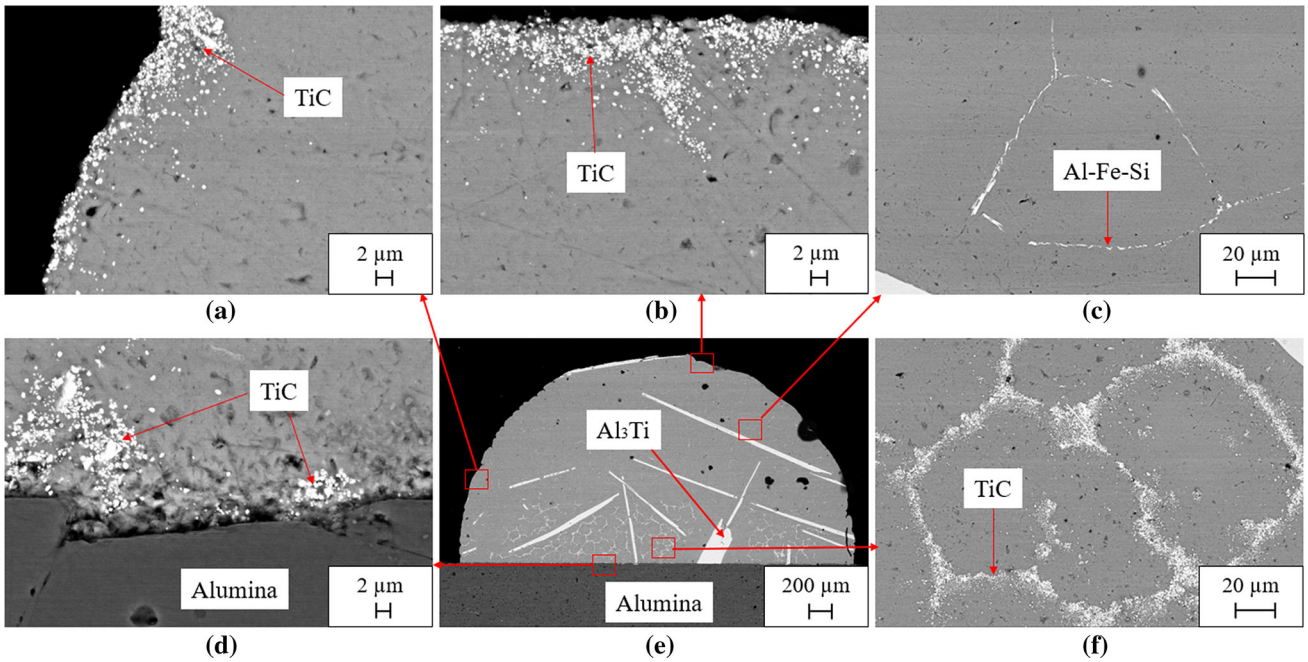

Fig. 7—The microstructure of Al-3Ti-0.15C master alloy on the alumina after 1 h holding at 1000 °C in high vacuum. (*a*) and (*b*) Magnified left and top side of the periphery of the droplet where TiC particles are agglomerated. (*c*) A magnified area in particle depletion zone where only Al-Fe-Si intermetallic phase is found along grain boundaries. (*d*) The interface between alumina substrate and Al, where TiC agglomerates and settles onto the substrate with no reaction layer observed. (*e*) Macrostructure of solidified sessile droplet on alumina. (*f*) A magnified area in particle sedimentation zone where massive TiC particles were agglomerated along grain boundaries.

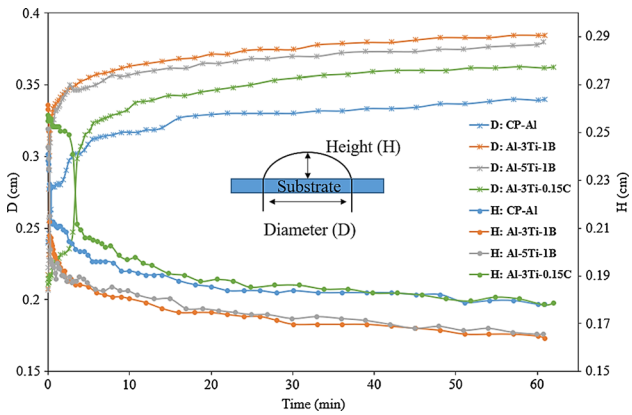

Fig. 8—Variation of base diameter (*D*), and droplet height (*H*) at 1000 °C in 1 × 10^{-3} Pa vacuum by the improved sessile drop method.

For a reactive system, a reaction layer will form at the liquid-solid interface. This would increase the wetting due to the alliance of the new layer to both liquid and solid. For example, Al_4C_3 layer forms for the Al-SiC system[20] and TiC layer forms at the interface between Al-3Ti melt and SiC substrate.[45] To check if any reaction layer has formed at the interface, the solidified droplet was first mechanically detached from the substrate and then the retained aluminum was etched off from the substrate by 10 pct NaOH solution. The interface structure is shown in Figure 9. As can be seen, a large fraction of grain refiner particles, TiB_2 and TiC, exist on the substrate. No reaction layer could be detected on the grain refiner particle-free areas in the substrate surface. This means that the lower contact angle of master alloys is not caused by the reaction layer formation for the present work. This is because most of the Ti content in the master alloys is occupied by the grain refiner particles. Thus, the concentration of free Ti atoms in the aluminum liquid is very low.

The viscosity, which is affected by alloy elements and intermetallic phases, influences the spreading of the liquid.[46] Higher viscosity usually causes a higher contact angle due to the slower spreading rate. Smaller droplet is also favorable for fast droplet spreading.[47] For the present work, the weights of samples were strictly controlled as 0.037 ± 0.003 g, which gives equal droplet size. It was reported that adding Al-5Ti-1B master alloy will increase the viscosity of Al melt at 720 °C.[48] It is expected that the grain refiner particles have the same effects at higher temperatures of 1000 °C and 1100 °C, therefore, a larger contact angle should be observed for the master alloy, which is not the case for the present work. Thus, the influence of viscosity on the wetting at such high temperatures for Al is probably neglectable in our case, and the reduction in contact angle for the master alloys is not supposed to be related to the viscosity change.

In the solidified master alloy droplets, there are a fraction of large Al_3Ti particles, in addition to the TiB_2 particles in Al-Ti-B, and TiC particles in Al-Ti-C. The surplus Ti contents in the alloys (more than necessary to form TiB_2 and TiC particles) reacts with Al, forming Al_3Ti. The TiB_2 and TiC particles are very stable at high temperatures and can survive at the test temperatures in

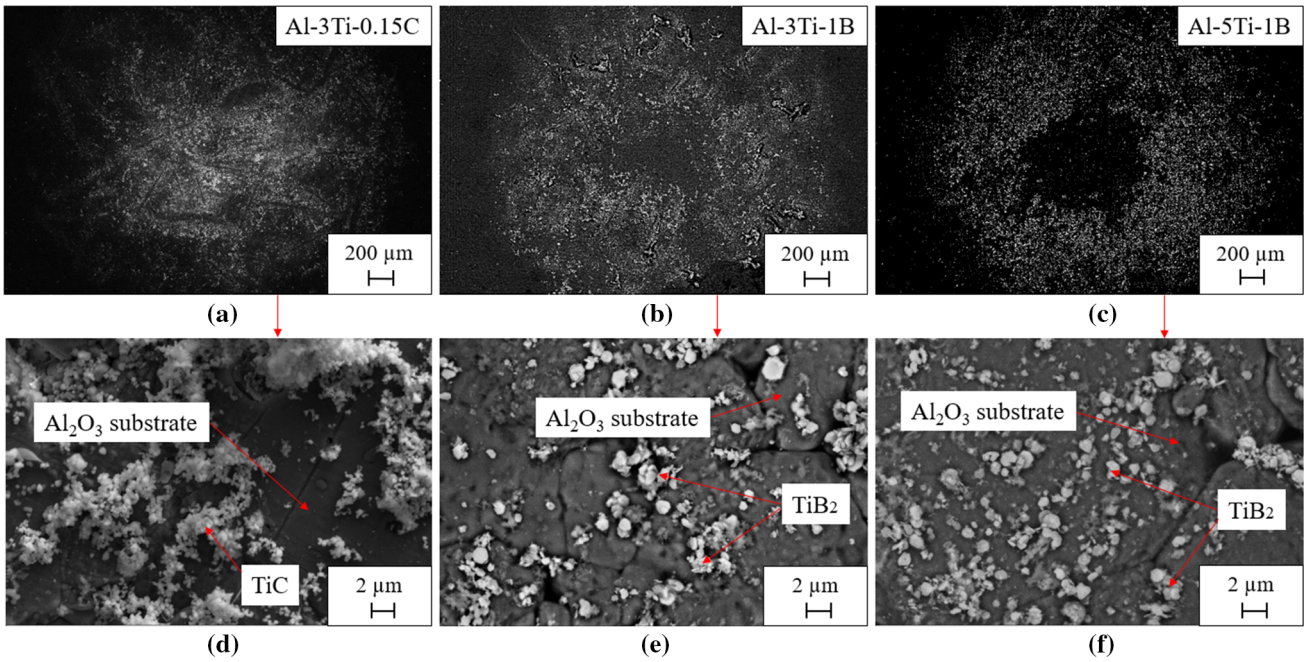

Fig. 9—Microstructure of the interface between grain refiner master alloy droplets and the substrate, after the solidified droplets were removed by mechanical detaching and chemical etching. (*d*) to (*f*) are the magnified pictures of (*a*) to (*c*), respectively. Only deposition of grain refiner particles while no reaction layer was detected.

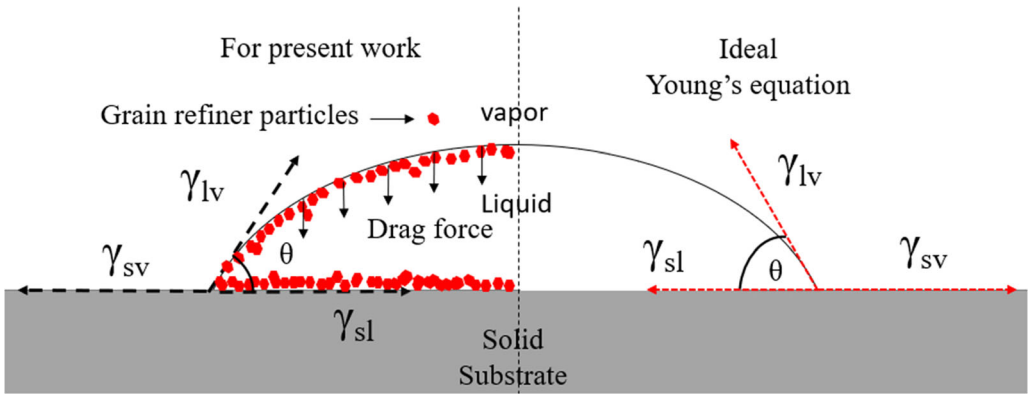

Fig. 10—Contact angle of a liquid droplet on the substrate in wetting equilibrium for an ideal situation and present work.

the present work. On the other hand, the Al_3Ti intermetallic phase cannot. Based on the Al-Ti phase diagram calculated by Thermo-Calc®, the Al_3Ti phase does not exist at 1100 °C for any of the used grain refiner master alloys, while it can exist in Al-5Ti-1B and Al-3Ti-0.15C alloy at 1000 °C. This indicates that the Al_3Ti phase found in the sample after conventional sessile drop test at 1100 °C should be formed during the solidification process and this phase should not be responsible for the contact angle reduction.

During wetting test, an equilibrium state will be achieved among liquid droplet, solid substrate, and the surrounding vacuum (with an extremely low pressure of gas atmosphere) as shown in Figure 10. This relationship can be expressed by Young's equation:

$$\cos(\theta) = \frac{\gamma_{sv} - \gamma_{sl}}{\gamma_{lv}}, \qquad [1]$$

where γ is the interfacial tension. Subscripts s, l, v refer to the solid, liquid, and vapor phases, and θ is the contact angle.

For a given value of γ_{lv}, the contact angle decreases when the γ_{sl} decreases or γ_{sv} increases, which gives improved wettability between the solid and the liquid phase.

The high contact angle between Al and alumina in literature[29–38] indicates a large γ_{sl}. However, the γ_{sl} between aluminum and TiC or TiB_2 is much smaller as inferred from the good wettability.[27,28,49] Since the sedimentation of TiB_2 and TiC particles at the bottom

of the droplets, which covers a large fraction of the interface between the droplet and substrate (Figures 6 and 7), the interface tension γ_{sl} between Al and alumina is partly changed to the γ_{sl} between grain refiner particles and Al. This results in a decrease in the solid-liquid interfacial energy which gives a lower contact angle. In addition, the particles agglomerating at the droplet surface also plays an important role in the contact angle reduction. The interface tension between liquid and vapor, γ_{lv}, influences the height of the droplet. Since the density of TiB_2 and TiC particles are higher than that of liquid aluminum, an agglomeration of the particles at the surface of the droplet will exert a dragging force to reduce the height of the droplet. As a consequence, the effective γ_{lv} in Eq. [1] will be reduced, which will cause a further decrease in contact angle. For the conventional sessile drop test, the Al-Ti-C and Al-Ti-B master alloys show a very similar contact angle to alumina substrate. However, with higher accuracy, the improved sessile drop test shows that the Al-Ti-B master alloys have a lower contact angle than Al-Ti-C. This may be attributed to the difference in the volume fraction of grain refiner particles in the two different types of master alloys. The TiB_2 and TiC contained in the master alloys are corresponding 3.2 wt pct, and 0.07 wt pct for Al-Ti-B (both Al-3Ti-1B and Al-5Ti-1B) and Al-3Ti-0.15C master alloys, respectively. Also, the density of the TiC particles settled on the substrate surface is lower than that of TiB_2 particles (Figures 6(d) and 7(d)). Furthermore, the size of TiB_2 particles is much larger than TiC, which may also increases the drag force and caused a lower contact angle.

B. *Contact Angle Evolution During Wetting Test*

The removal of oxide skin at the surface of the droplets is believed to have a major influence on contact angle evolution. The measured contact angle between Al on Al_2O_3 in literature lies between 67 to 110 and 60 to 97 deg[30–34] at 1000 °C and 1100 °C, respectively. This large scattering of the measured contact angle data is mainly ascribed to the existence of oxide skin on the droplets, particularly at relatively lower temperatures ($T < 1000$ °C).[32] The original thickness of the oxide skin can be affected by environmental conditions, sample purity, pre-treatment, vacuum status, *etc*. In an Al-Al_2O_3 system, the contact angle decreases with the thickness reduction of this oxide skin layer. The removal of oxide layer can be evaluated by Reaction [2] with fast heating.[31] At 1000 °C, the critical equilibrium partial pressure of Al_2O according to Reaction [2] is 4.3 Pa, under which, the oxidation layer on Al surface will be removed. For the present study, both temperature and vacuum state fulfilled the requirement for such a reaction to happen.

$$4Al(l) + Al_2O_3(s) = 3Al_2O(g). \quad [2]$$

For the present case, the master alloys were observed to have a faster deoxidation process than CP-Al in all cases, as illustrated in Figures 4 and 5. This is ascribed to the grain refiner particles distributing along the droplet surface. Since the grain refiner particles are heavier than the Al melt, sedimentation of the particles happens during the wetting test, which resulted in the particle depletion zone in the upper part of the droplets. However, the particles at the periphery of the droplet kept staying at the surface, implying that these particles have been trapped by the surface oxide layer of the droplet. This indicates a strong adherence exists between the surface aluminum oxide film and the grain refiner particles. Meanwhile, the particles agglomerated along grain boundaries in the particle sedimentation zone is a result of solidification frontline accumulation.[50] The adherence of grain refiner particles on the oxide films may have also the influence on enhancing the rapture of the oxide skin at the beginning of wetting test, due to the dragging force of the particles. In the late stage of wetting test, the existence of a dense population of grain refiner particles on the oxide skin will slow down the re-oxidation by hindering the transportation of fresh Al atoms to the surface.

Figure 11 presents a schematic drawing to show the behavior of grain refiner particles in Al droplets during wetting experiments. In the beginning, Al droplet is covered with relatively thick oxide skin, most of which is from the original oxide layer at the surface of solid sample. Inside the droplet, the floating grain refiner particles move around due to the internal convection of liquid. Some of the particles move to the surface oxide skin and being captured (Figure 11(a)). During heating, rupture of the thick oxide layer will happen due to the incompatible expansion between liquid and oxide layer. The grain refiner particles adhered to the oxide layer can

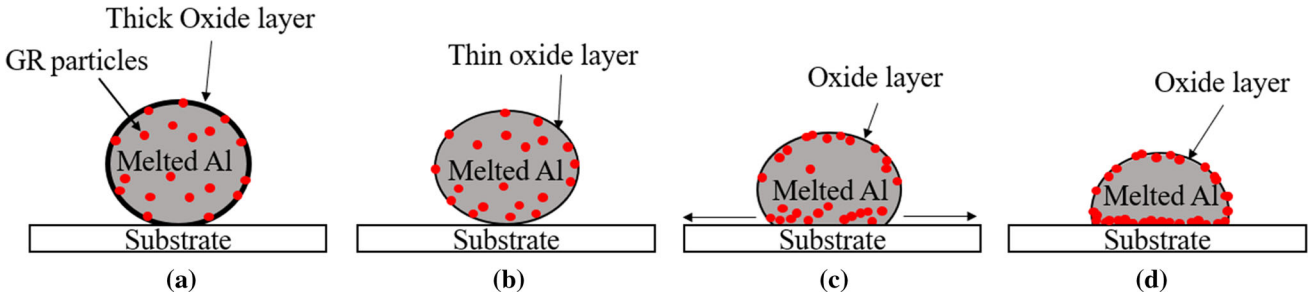

Fig. 11—An illustration of wetting of a substrate by an Al alloy containing grain refiner (GR) particles: (*a*) Alloys melt and GR particles move towards the surface and attach to the oxide layer which may help deoxidation. (*b*) GR particles further move towards the oxide skin. (*c*) Uncaptured GR particles start to settle. (*d*) The GR particles partly deposit on the substrate and partly chain on the metal surface.

help the oxide rupture process by impingement (Figure 11(b)). Once the thick oxide layer is ruptured, the liquid metal can spread more freely, and cause a sharp reduction in contact angle (Figure 11(c)). This spreading may become faster due to the downward dragging force of grain refiner particles on the oxide skin. It is important to mention that the Al melt will still reoxidize[39] in the high vacuum in the present wetting experiments, even though the pumping system would take away the Al_2O gas continuously until a dynamic equilibrium between re-oxidization and deoxidization is achieved. The grain refiner particles along the oxide skin will also hinder the transportation of Al atoms to the surface. As a result, the balanced thickness of the oxide layer should be thinner for master alloys than CP-Al. Thereby, a better wetting is expected. In the end, a fraction of grain refiner particles have adhered to the oxide skin, and the rest of the particles agglomerate and settle down onto the substrate surface (Figure 11(d)). With a large fraction of grain refiner particles distributed on the substrate, the wetting system has changed from Al—alumina to Al—grain refiner particles—alumina. The agglomeration of grain refiner particles at the triple line (Figure 6(a)) also helped to improve the wettability between the melt and substrate (lower the contact angle).

C. *Influence of Grain Refiner Particles on Filtration*

It has to be mentioned that master alloys were directly used for wetting tests in the current work, while the addition level of grain refiner master alloys is usually 0.5 to 1 kg/ton in cast house. The total number of the grain refiner particles in the master alloy is about three orders of magnitude higher than in the commercial alloys inoculated by master alloys. Thus, the influence of grain refiner particles on the contact angle between commercial Al melt and alumina substrate can be expected to be much smaller. On the other hand, the lower contact angle between the melts of master alloys and alumina is mainly due to the adherence of grain refiner particles to the oxide skin of droplets. However, during the real filtration process, the aluminum melt is continuous while free droplet surface with oxide skins may not exist. In the flowing melt, the sedimentation of grain refiner particles at the surface of porous wall filter may also be difficult. It is rather safe to propose that the influences of grain refiner particles on the wetting behavior filter to aluminum melt might be negligible in the industrial cases. Therefore, the reduced filtration efficiency by grain refiner particles should not be ascribed to the wetting angle reduction. However, the finding of the strong adherence between grain refiner particles and aluminum oxide film in this work may help to explore the reason why grain refiner particles reduce the filtration efficiency, because oxide film is one of the main sources of inclusion in aluminum melt. Research on the interaction between aluminum oxide films and grain refiner particles in aluminum melt during filtration is ongoing and will be reported in future work.

V. CONCLUSIONS

The wettability between CP-Al, master alloys Al-3Ti-1B, Al-5Ti-1B, and Al-3Ti-0.15C and alumina substrate was tested by both conventional sessile drop method and improved sessile drop method. The major conclusions are summarized as follows:

1. The master alloys show a better wettability (lower contact angle) towards alumina substrate than CP-Al. This is ascribed to the existence of a large amount of grain refiner particles, TiB_2 and TiC, in the master alloys.
2. Strong sedimentation of the grain refiner particles happens in the droplet of master alloys during wetting test, due to the density difference between the particles and Al melt. The sedimentation of the particles on the surface of alumina substrate decreases the solid-liquid interfacial energy, and therefore, reducing the contact angle.
3. It is found that the oxide skin of the droplets has a strong adherence to the grain refiner particles. A large fraction of the particles are agglomerated along the oxide skin of the droplets, which has also the influence of reducing the contact angle between master alloy melt and alumina substrate.
4. The reduction in the contact angle between grain refiner master alloy melts and the alumina substrate with increasing holding time during both improved and conventional sessile drop wetting tests is significantly faster than that of CP-Al. This is also due to the agglomeration of grain refiner particles on the oxide skin, which enhances the rapture of the thick oxide skin in the early stage of wetting while reduces the thickness of the re-oxidized skin in the late stage.

VI. FUTURE WORK

The observation of the strong adherence between grain refiner particles and oxide films is particularly interesting and its effects on the filtration efficiency of grain refined aluminum alloys is worth for more detailed investigation. The research work is ongoing, and the results will be reported in late publications.

ACKNOWLEDGMENTS

This research was carried out as part of the Norwegian Research Council (NRC) - funded BIA-IPN Project (256724/O20) SmartAl. It includes the following partners: Hydro Aluminum AS, Hydal Aluminum Profiler AS, Hycast AS, Ekornes ASA, NTNU and SINTEF. Funding by the industrial partners and NRC is gratefully acknowledged.

FUNDING

Open Access funding provided by NTNU Norwegian University of Science and Technology (incl St. Olavs Hospital - Trondheim University Hospital).

REFERENCES

1. L.N.W. Damoah and L. Zhang: *Acta Mater.*, 2011, vol. 59, pp. 896–913.
2. H.-Y. Hwang, C.-H. Nam, Y.-S. Choi, J.-H. Hong, and X. Sun: *China Foundry*, 2017, vol. 14, pp. 216–25.
3. S. Bao, M. Syvertsen, A. Kvithyld, and T. Engh: *Trans. Nonferrous Metal. Soc.*, 2014, vol. 24, pp. 3922–28.
4. G. Song, B. Song, Z. Yang, Y. Yang, and J. Zhang: *Metall. Mater. Trans. B*, 2016, vol. 47B, pp. 3435–45.
5. H. Görner: Ph.D. thesis, Norwegian University of Science and Technology, 2009.
6. L.N.W. Damoah and L. Zhang: *Metall. Mater. Trans. B*, 2010, vol. 41B, pp. 886–907.
7. E. Laé, H. Duval, C. Rivière, P. Le Brun, and J.-B. Guillot: *Essential Readings in Light Metals: Volume 3 Cast Shop for Aluminum Production*, ed. John F. Grandfield and Eskin Dmitry G., Springer, Cham, 2016, pp. 285–90.
8. C. Voigt, B. Fankhänel, E. Jäckel, C.G. Aneziris, M. Stelter, and J. Hubálková: *Metall. Mater. Trans. B*, 2015, vol. 46B, pp. 1066–72.
9. J. Grandfield: *Light Metals*, Springer, Berlin, 2017, pp. 1429–34.
10. N.V. Buchilin, V.G. Maksimov, and V.G. Babashov: *Glass Ceram.*, 2015, vol. 72, pp. 246–52.
11. C. Conti and P. Netter: *Sep. Technol.*, 1992, vol. 2, pp. 46–56.
12. C. Voigt, B. Fankhänel, B. Dietrich, E. Storti, M. Badowski, M. Gorshunova, G. Wolf, M. Stelter, and C. Aneziris: *Metall. Mater. Trans. B*, 2020, vol. 51, pp. 2371–80.
13. N.G. Towsey, W. Schneider, and H.-P. Krug: *Aluminium Cast House Technology (Seventh Australasian Conference)*, ed. P.R. Whiteley, Wiley, New York, 2013, p 125.
14. J. Bäckman, I.L. Svensson, and Y. Maeda: *Influence of Filter on the Mould Filling of Aluminium Melts in Vacuum-Sealded Moulds*, Ingenjörshögskolan, Borås, 1999.
15. J. Desmoulins, H. Dhondt, and P. Netter: *J. Met.*, 1988, p. 36.
16. C. Voigt, E. Jäckel, F. Taina, T. Zienert, A. Salomon, G. Wolf, C.G. Aneziris, and P. Le Brun: *Metall. Mater. Trans. B*, 2017, vol. 48, pp. 497–505.
17. S. Bao, M. Syvertsen, A. Nordmark, A. Kvithyld, T. Engh, and M. Tangstad: *Light Metals* 2016, pp. 981–86.
18. S. Bao, K. Tang, A. Kvithyld, T. Engh, and M. Tangstad: *Trans. Nonferrous Metal. Soc.*, 2012, vol. 22, pp. 1930–38.
19. C. Voigt, L. Ditscherlein, E. Werzner, T. Zienert, R. Nowak, U. Peuker, N. Sobczak, and C.G. Aneziris: *Mater. Des.*, 2018, vol. 150, pp. 75–85.
20. S. Bao, A. Kvithyld, S. Gaal, T. Engh, and M. Tangstad: *Light Metals,* 2009, pp. 767–73.
21. C. Voigt, L. Ditscherlein, E. Werzner, T. Zienert, R. Nowak, U. Peuker, N. Sobczak, and C.G. Aneziris: *Light Metals,* 2019, pp. 1071–79.
22. C. Voigt, B. Dietrich, M. Badowski, M. Gorshunova, G. Wolf, and C.G. Aneziris: *Light Metals*, 2019, pp. 1063–69.
23. N. Towsey, W. Schneider, H.-P. Krug, A. Hardman and N.J. Keegan: *Continuous Casting*, ed. K. Ehrke and Schneider W., Wiley-VCH, New York, 2006, pp. 26–32.
24. N. Towsey, W. Schneider, H.-P. Krug, A. Hardman, and N.J. Keegan: *Essential Readings in Light Metals: Volume 3 Cast Shop for Aluminum Production*, ed. J.F. Grandfield and D.G. Eskin, Springer, Cham, 2016, pp. 291–95.
25. H. Duval, C. Rivière, E. Laé, P. Le Brun, and J.-B. Guillot: *Metall. Mater. Trans. B*, 2009, vol. 40, p. 233.
26. S. Ray, B. Milligan and N. Keegan: *Alum. Cast House Technol.,* 2005, pp. 1–12.
27. D.A. Weirauch, W.J. Krafick, G. Ackart, and P.D. Ownby: *J. Mater. Sci.*, 2005, vol. 40, pp. 2301–06.
28. Q. Lin, P. Shen, L. Yang, S. Jin, and Q. Jiang: *Acta Mater.*, 2011, vol. 59, pp. 1898–1911.
29. H. John and H. Hausner: *J. Mater. Sci. Lett.*, 1986, vol. 5, pp. 549–51.
30. S. Wolf, A. Levitt, and J. Brown: *Chem. Eng. Prog.*, 1966, vol. 62, pp. 74–78.
31. S. Bao, K. Tang, A. Kvithyld, M. Tangstad, and T.A. Engh: *Metall. Mater. Trans. B*, 2011, vol. 42B, pp. 1358–66.
32. P. Shen, H. Fujii, T. Matsumoto, and K. Nogi: *J. Am. Ceram. Soc.*, 2004, vol. 87, pp. 2151–59.
33. P. Shen, H. Fujii, T. Matsumoto, and K. Nogi: *Scripta Mater.*, 2003, vol. 48, pp. 779–84.
34. Y.V. Naidich, Y.N. Chubashov, N.F. Ishchuk, and V.P. Krasovskii: *Sov. Powder Metall. Met. Ceram.*, 1983, vol. 22, pp. 481–483.
35. D.-J. Wang and S.-T. Wu: *Acta Metall. Mater.*, 1994, vol. 42, pp. 4029–34.
36. A.J. Klinter, G. Mendoza-Suarez, and R.A.L. Drew: *Mater. Sci. Eng. A*, 2008, vol. 495, pp. 147–52.
37. V. Laurent, D. Chatain, C. Chatillon, and N. Eustathopoulos: *Acta Metall.*, 1988, vol. 36, pp. 1797–1803.
38. N. Shinozaki, K. Mukai, and T. Fujita: *Metall. Mater. Trans. B*, 2002, vol. 33B, pp. 506–09.
39. N. Sobczak, R. Nowak, W. Radziwill, J. Budzioch, and A. Glenz: *Mater. Sci. Eng. A*, 2008, vol. 495, pp. 43–49.
40. P. Shen, H. Fujii, and K. Nogi: *Acta Mater.*, 2006, vol. 54, pp. 1559–69.
41. P. Shen, H. Fujii, T. Matsumoto, and K. Nogi: *Acta Mater.*, 2003, vol. 51, pp. 4897–4906.
42. P. Shen, H. Fujii, T. Matsumoto, and K. Nogi: *Acta Mater.*, 2004, vol. 52, pp. 887–98.
43. J. Lee, A. Kiyose, S. Nakatsuka, M. Nakamoto, and T. Tanaka: *ISIJ Int.*, 2004, vol. 44, pp. 1793–99.
44. R.E. Honig and R.C.O.A.R.L. Division: *Vapor Pressure Data for the More Common Elements*, David Sarnoff Research Center, Princeton, 1957.
45. Q. An, X.-S. Cong, P. Shen, and Q.-C. Jiang: *J. Alloys Compd.*, 2019, vol. 784, pp. 1212–20.
46. G. Kumar and K.N. Prabhu: *Adv. Colloid Interface Sci.*, 2007, vol. 133, pp. 61–89.
47. C.W. Extrand: *J. Colloid Interface Sci.*, 1993, vol. 157, pp. 72–76.
48. L. Yu and X. Liu: *J. Alloys Compd.*, 2006, vol. 425, pp. 245–50.
49. A. Contreras, C.A. León, R.A.L. Drew, and E. Bedolla: *Scr. Mater.*, 2003, vol. 48, pp. 1625–30.
50. P.L. Schaffer and A.K. Dahle: *Mater. Sci. Eng. A*, 2005, vols. 413–414, pp. 373–78.